Lattice-Directed Formation of Covalent and Organometallic Molecular Wires by Terminal Alkynes on Ag Surfaces

Jing Liu,[†] Qiwei Chen,[†] Lianghong Xiao,[‡] Jian Shang,[†] Xiong Zhou,[†] Yajie Zhang,[†] Yongfeng Wang,[*,§] Xiang Shao,[∥] Jianlong Li,[†] Wei Chen,[⊥,#] Guo Qin Xu,[⊥,#] Hao Tang,[¶] Dahui Zhao,[*,‡] and Kai Wu[*,†,#]

[†]BNLMS, College of Chemistry and Molecular Engineering, [‡]MOE Key Lab of Polymer Chemistry & Physics, College of Chemistry and Molecular Engineering, and [§]Key Laboratory for the Physics and Chemistry of Nanodevices, Department of Electronics, Peking University, Beijing 100871, China, [∥]Department of Chemical Physics, School of Chemistry and Materials Science, University of Science and Technology of China, Hefei 230026, China, [⊥]Department of Chemistry, National University of Singapore, Singapore 117543, [#]SPURc, 1 CREATE Way, #15-01, CREATE Tower, Singapore 138602, and [¶]Groupe Matériaux Crystallins sous Contrainte, CEMES-CNRS, Boîte Postale 94347, 31055 Toulouse, France

ABSTRACT Surface reactions of 2,5-diethynyl-1,4-bis(phenylethynyl)-benzene on Ag(111), Ag(110), and Ag(100) were systematically explored and scrutinized by scanning tunneling microscopy, molecular mechanics simulations, and density functional theory calculations. On Ag(111), Glaser coupling reaction became dominant, yielding one-dimensional molecular wires formed by covalent bonds. On Ag(110) and Ag(100), however, the terminal alkynes reacted with surface metal atoms, leading to one-dimensional organometallic nanostructures. Detailed experimental and theoretical analyses revealed that such a lattice dependence of the terminal alkyne reaction at surfaces originated from the matching degree between the periodicities of the produced molecular wires and the substrate lattice structures.

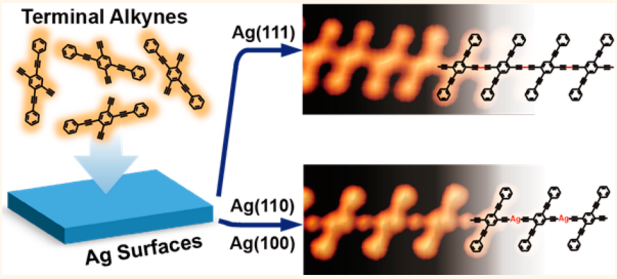

KEYWORDS: terminal alkynes · Ag single crystals · surface reaction · molecular wires · lattice match

Preparation of robust nanostructures at the surface by a bottom-up approach has received great attention in the past decade[1−6] due to its wide applications in fabricating functional nanomaterials and high-performance molecular electronic devices.[7−10] A variety of chemical precursors have been explored, aiming at fabricating both covalent and organometallic nanostructures. To prepare low-dimensional and functional covalent polymers, Ullmann coupling of halides,[2,4,5,11−15] dehydration and esterification of boronic esters,[16] dehydrogenative coupling of alkanes,[17] N-heterocyclic carbene dimerization of pyridines or pyrimidines,[18] chain polymerization of diynes,[19−21] Bergman cyclization of enediynes,[22] and the like have been extensively employed and explored. Meanwhile, organometallic nanostructures have also been achieved by reactions between metal atoms and molecules with labile groups such as bromo[23−25] and proton.[26−28] Most precursors react to yield a major product even under different reaction conditions. However, terminal alkynes, another family of precursor candidates for surface reactions, have been reported to adopt several reaction pathways and thus result in different products. Glaser coupling,[29,30] the homocoupling between terminal alkynes, has been appreciated as a promising route to construct graphdiyne-related nanostructures on surfaces.[31−37] Apart from Glaser coupling, terminal alkynes can form nanostructures *via* cyclotrimerization[38,39] and other reactions,[33,34,40] as well. In addition, terminal alkynes can react with metal atoms to form organometallic species at surfaces,[34,39] even though these species are only observed as segments or oligomers involving several molecules. Therefore, in terms of the complexity of the surface reactions of terminal alkynes, efficiently tuning

* Address correspondence to kaiwu@pku.edu.cn, yongfengwang@pku.edu.cn, dhzhao@pku.edu.cn.

Received for review March 25, 2015 and accepted May 19, 2015.

Published online May 19, 2015
10.1021/acsnano.5b01803

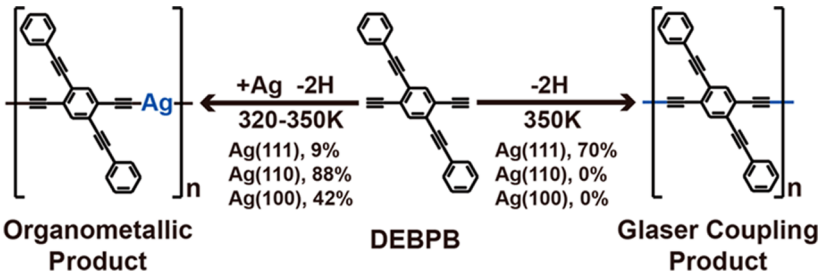

Scheme 1. Main reaction pathway of DEBPB on Ag(111), Ag(110), and Ag(100).

the reaction pathways and the product selectivity remains a great challenge. Two major strategies have been adopted to control the reactions of terminal alkynes either by changing the precursor backbone or by employing different substrates, that is, various metal substrates or different lattice planes of the same metal substrate. In the former strategy, by using D_{3h} terminal alkyne precursors, Liu and co-workers have achieved cyclotrimerized frameworks with a 75% productivity on Au(111),[38] while the linear precursors with alkyl side groups were used to mainly achieve the Glaser coupling under similar conditions.[33] In the latter strategy, Gao *et al.* have explored the effect of different metal substrates on the surface reactions of terminal alkynes and found that Ag(111) provided the highest yield of Glaser coupling while Au(111) and Cu(111) triggered side reactions.[33,34] Various lattice planes of the same metal substrate, another significant structural feature, are much less investigated even though they might play an important role in controlling the surface reactions of terminal alkynes. For instance, Gao and coworkers[33] observed a selectivity toward Glaser coupling on Au(100) worse than that on Au(111), while Cirera *et al.*[36] reported a selectivity for the Glaser coupling reaction on Ag(877) higher than that on Ag(111).

In this study, different Ag lattice planes were used to steer the surface reactions of terminal alkyne. The terminal alkyne precursor employed was 2,5-diethynyl-1,4-bis(phenylethynyl)benzene (DEBPB), and its reactions on Ag(111), Ag(110), and Ag(100) were studied by ultrahigh vacuum (UHV) scanning tunneling microscopy (STM), molecular mechanics (MM) simulations, and density functional theory (DFT) calculations. A significant effect of the substrate lattice structure on the reaction pathway and product selectivity of DEBPB was identified. Different major reactions took place on Ag(111) and Ag(110)/Ag(100), leading to distinct main products at similar reaction temperatures (Scheme 1). On Ag(111), most DEBPB molecules underwent Glaser coupling to form one-dimensional (1D) covalent molecular chains. On Ag(110) and Ag(100), however, the reaction between terminal alkynes and metal atoms took place to produce 1D organometallic chains. These results indicate that the surface reactions of the terminal alkynes can be efficiently tuned by using different lattice planes of the same metal substrate.

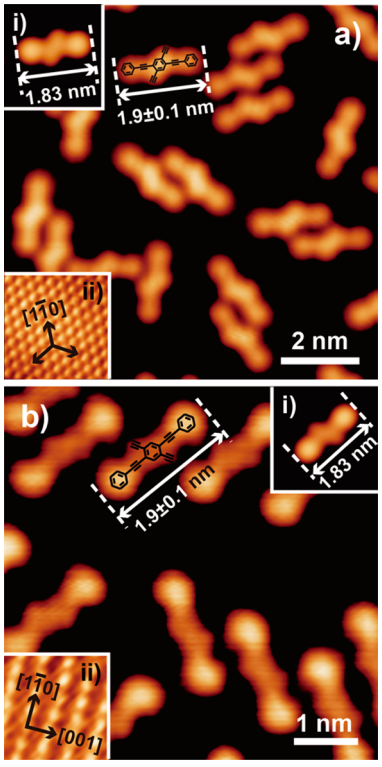

Figure 1. (a) STM images of the DEBPB molecules on Ag(111) (scanning bias = 0.01 V, feedback current = 100 pA). The molecules are deposited onto the substrate, which is held at about 100 K. The chemical structure of DEBPB is superimposed, and its measured length is indicated. Inset (i): Simulated STM of a DEBPB molecule on Ag(111) (0.1 V, 100 pA) with its calculated length marked. Inset (ii): High-resolution STM image of the Ag(111) surface lattice structure (0.01 V, 70 pA). (b) STM images of the DEBPB molecules on Ag(110) (0.01 V, 100 pA) under the same deposition conditions as in (a). The chemical structure of DEBPB is superimposed, and its measured length is indicated. Inset (i): Simulated STM of a DEBPB molecule on Ag(110) (0.1 V, 100 pA) with its calculated length. Inset (ii): High-resolution STM image of the Ag(110) surface lattice structure (0.01 V, 120 pA).

RESULTS

DEBPB Monomers on Ag(111) and Ag(110). Panels a and b of Figure 1 display representative STM images of the molecular monomers on Ag(111) and Ag(110), respectively, after deposition of the DEBPB molecules onto the substrates kept at about 100 K and subsequent annealing at room temperature for 10 min. The DEBPB molecules were sparsely distributed on both

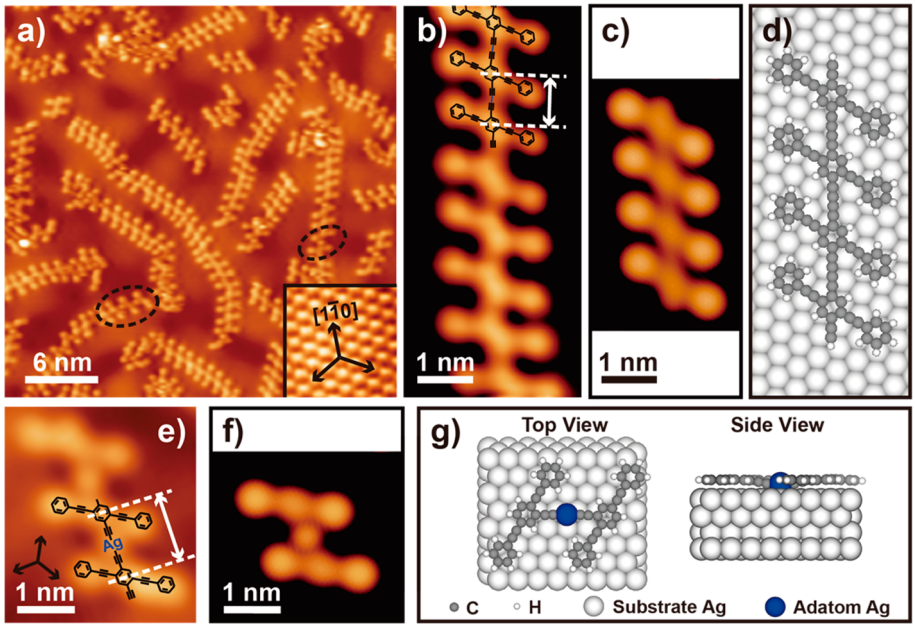

Figure 2. (a) STM image of produced molecular chains on Ag(111) after annealing at about 350 K (0.01 V, 60 pA). Inset: High-resolution STM image of the Ag(111) surface lattice structure (0.01 V, 70 pA). (b) High-resolution STM image of a Glaser-coupled covalent chain (0.01 V, 150 pA) with the chemical structure superimposed. The distance measured between the centers of two adjacent molecules is highlighted by the white arrow. (c) Simulated STM image of a Glaser-coupled covalent tetramer on Ag(111) (0.1 V, 100 pA). (d) Optimized molecular model of a Glaser-coupled covalent tetramer on Ag(111). (e) High-resolution STM image of an organometallic trimer (0.01 V, 150 pA) with the chemical structure superimposed. The distance measured between the centers of two adjacent molecules is highlighted by the white arrow. [1$\bar{1}$0] and its two other equivalent directions of the Ag(111) substrate are marked by the black arrows. (f) Simulated STM image of a simplified organometallic dimer on Ag(111) (0.1 V, 100 pA). (g) Top and side views of the molecular model of a simplified organometallic dimer on Ag(111).

substrates without formation of any ordered structures and looked like a crisscross in the STM image. The long side of the crisscross was measured to be 1.9 ± 0.1 nm on both Ag(111) and Ag(110) substrates, in accordance with the calculated length of the DEBPB backbone, 1.83 nm. The short side of the crisscross, on the other hand, showed the orientation of two-terminal alkynyl groups, as depicted by the superimposed chemical structures in Figure 1a,b. Simulated STM images of the DEBPB monomers on Ag(111) and Ag(110) (Figure 1a-i and b-i) are in excellent agreement with the experimental ones.

Covalent Chains Formed on Ag(111) *via* Glaser Coupling. After deposition and subsequent annealing at about 350 K, the Ag(111) substrate was covered by 1D molecular chains of different length (Figure 2a) which were formed by covalent homocoupling between the DEBPB molecules. High-resolution STM image of an individual molecular chain (Figure 2b) unambiguously showed connections between the terminal alkynyl groups of two neighboring DEBPB molecules. The distance between the centers of two adjacent molecules in a chain, marked by the white arrow in Figure 2b, was measured to be 0.94 ± 0.04 nm. This value was in accordance with the calculated distance, about 0.91 nm, between the centers of two DEBPB molecules connected with the C−C covalent bond formed *via* the Glaser coupling. Moreover, the simulated STM image of a covalent-bonded tetramer (Figure 2c) according to the optimized model (Figure 2d) was in agreement with the experimentally observed 1D molecular chains. These facts suggested that the 1D molecular chains on Ag(111) were formed *via* the Glaser coupling between the DEBPB molecules, as indicated by the superimposed chemical structure in Figure 2b, where the terminal alkynyl groups of adjacent DEBPB molecules in the chains were connected by covalent C−C bonds. The Glaser-coupled nanostructures were the main product on Ag(111) with a relatively high productivity of 70% (Supporting Information).

In addition to the covalent-bonded molecules, some segments on Ag(111), such as those marked by black dashed circles in Figure 2a, were somewhat different. As shown in the high-resolution STM image of one segment (Figure 2e), a round dot between two neighboring molecules could be clearly discerned, implying the involvement of the Ag adatoms in this structure. The distance between the centers of two adjacent DEBPB molecules, as marked by the white arrow in Figure 2e, was measured to be 1.23 ± 0.05 nm, which is larger than that between the centers of two covalently coupled molecules. This value was actually in good agreement with the calculated one between the centers of two simplified DEBPB molecules (about 1.21 nm) that are connected to each other through

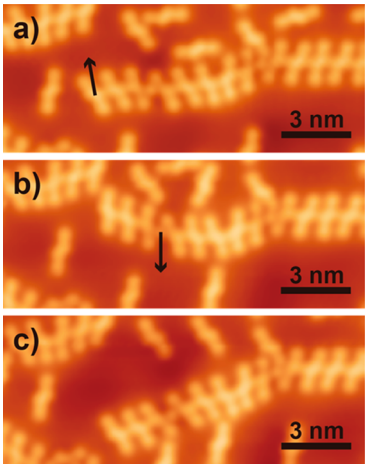

Figure 3. (a) Lateral tip manipulation of the molecular chain on Ag(111) at its ending position along the direction marked by the black arrow (0.10 V, 100 pA). (b) STM image of the same area after the first tip manipulation (0.10 V, 100 pA). A second trial is then performed at the Ag atom in the chain along the direction marked by the black arrow. (c) STM image of the same area after the second tip manipulation (0.10 V, 100 pA).

bonding with a silver adatom, as shown by models in Figure 2g. Furthermore, the simulated STM image of an organometallic dimer (Figure 2f) according to the optimized models (Figure 2g) was in great agreement with the experimental one. These comparisons led to the conclusion that these special structures were organometallic species, as shown by the superimposed chemical structure in Figure 2e, formed by the reaction between the DEBPB molecules and Ag atoms.

Lateral STM tip manipulation on the chains (Figure 3) was conducted to verify that the molecules in the 1D chains were indeed chemically bonded. Tip manipulations at the end of a 1D molecular chain (Figure 3a) and at the Ag atom in the organometallic segment of the chain (Figure 3b) were sequentially carried out, as indicated by the black arrows in Figure 3a,b. In each step of the tip manipulation, the 1D chain moved or bent as a whole without breakage. These manipulation experiments demonstrated that the molecules and silver atoms in the 1D chains were strongly bonded and possessed an appreciable flexibility reported in other systems.[36,41] Meanwhile, the fact that the 1D molecular chains could be easily moved as a whole suggested a weak interaction between the substrate and the chains, which was further supported by the disordered arrangement and random orientation of the 1D molecular chains on Ag(111) (Figure 2a).

Organometallic Chains Formed on Ag(110) *via* the Reaction between DEBPB Molecules and Ag Adatoms. In contrast, after being annealed at about 350 K, the Ag(110) substrate was mainly covered by parallel chains with a few oligomers of byproducts trapped between (Figure 4a). The 1D chains were highly oriented and exclusively extended along the [001] direction of the Ag(110) substrate. High-resolution STM image of the 1D chains (Figure 4b) achieved with a CO-modified tip (Supporting Information) clearly showed that a round dot was located between two adjacent molecules and connected by the alkynyl groups of nearby molecules, indicating the involvement of Ag atoms in the chains, just as in the case for organometallic segments on Ag(111). The distance between the centers of two neighboring molecules (1.24 $\pm$ 0.02 nm) was in agreement with the calculated distance between the centers of two DEBPB molecules connected by a Ag atom (1.22 nm), as shown by the models in Figure 4e. Moreover, the simulated STM image of an organometallic tetramer (Figure 4c) according to the optimized model (Figure 4e) agreed well with the experimental result. These results substantiated that the 1D chains on Ag(110) were organometallic species, as shown by the superimposed chemical structure in Figure 4b, formed by the reaction between the DEBPB molecules and Ag adatoms. The 1D organometallic chains were the main product on Ag(110) with a productivity of 88% (Supporting Information), while no Glaser coupling product was observed.

More interestingly, different from the organometallic structures synthesized by surface reaction of alkyl bromides *via* the Ullmann coupling at higher temperatures,[23,25,42,43] no Glaser coupling product formed by the DEBPB molecules was identified even after sequential thermal treatment of the sample up to about 450 K (Supporting Information).

DISCUSSION

The relatively high selectivity toward Glaser coupling on Ag(111) in this work is not an exception because Ag(111) has been experimentally[33,34] and theoretically[34] proven to be the best substrate for Glaser coupling with minimized side reactions with respect to the Au(111) and Cu(111) substrates due to its appropriate interaction with the alkynyl groups. Moreover, the DEBPB precursor possesses a rigid backbone where the *ortho* substituents, phenylethynyls in the central benzyl core, introduce steric hindrance that prevents side reactions involving three or more molecules.[33] As a result, a relatively high selectivity of the Glaser coupling reaction (70%, Supporting Information) on Ag(111) was achieved, compared with previous reports.[33,34]

Unlike the generally observed Glaser coupling products, the large-scale organometallic reactions between the terminal alkynes and metal atoms into metal−acetylides have rarely been reported. The organometallic products only appeared as segments or oligomers involving several molecules.[34,39] However, in our study, massive formation of highly oriented 1D organometallic chains with a productivity of 88% (Supporting Information) was achieved on Ag(110). Generally, the selectivity of an on-surface reaction is determined by both the reaction mechanism (kinetics)

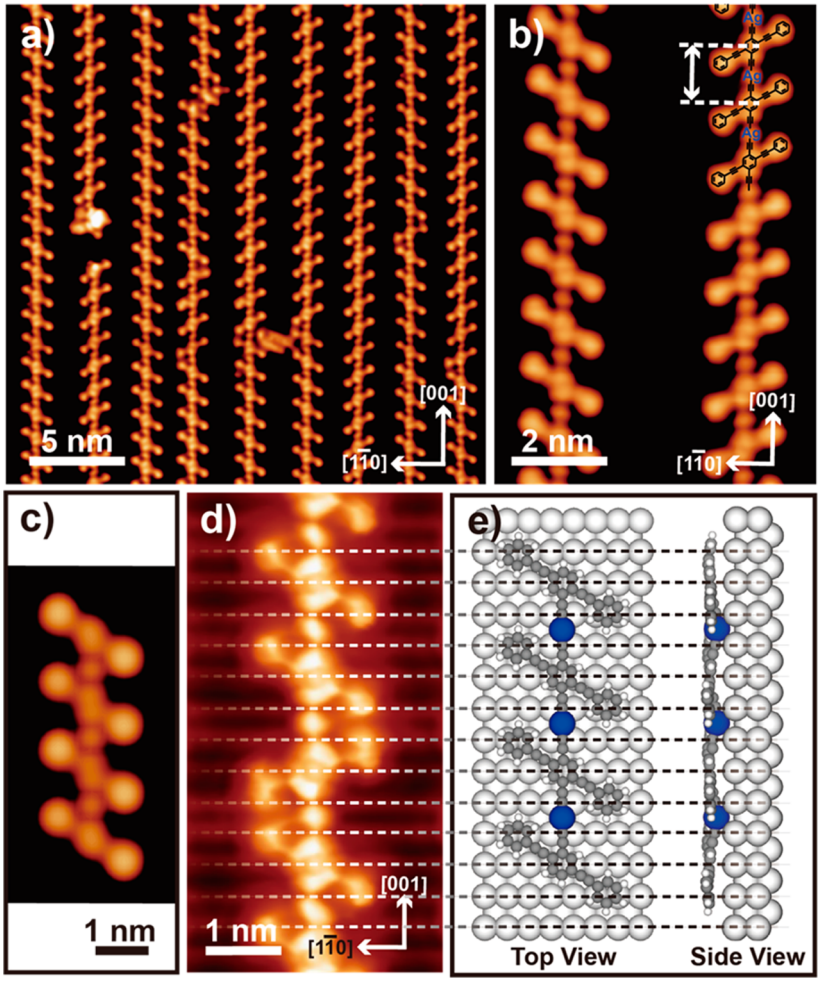

Figure 4. (a) STM image of an array of highly oriented organometallic chains on Ag(110) after annealing at about 350 K (0.01 V, 100 pA). (b) High-resolution STM image of two organometallic chains achieved by using a CO-modified tip (0.05 V, 100 pA) with the proposed chemical structure superimposed. The distance measured between the centers of two adjacent molecules is highlighted by the white arrow. (c) Simulated STM image of a simplified organometallic tetramer on Ag(110) (0.1 V, 100 pA). (d) High-resolution STM image of an organometallic chain achieved by using a CO-modified tip with the lattice stripes along the [1$\bar{1}$0] direction of the Ag(110) substrate in constant height mode (0.01 V, 100 pA). (e) Top and side views of the molecular model of a simplified organometallic tetramer on Ag(110). The lattice stripes along the [1$\bar{1}$0] direction of the Ag(110) substrate are highlighted by dashed lines in (d) and (e).

and the adsoprtion energy of particular product(s) on surfaces (thermodynamics). Theoretical studies[34,35] on the reaction of terminal alkynes on Ag(111) suggest that butadiyne, which would lead to covalent products rather than metal−acetylide species, is likely to be the intermediate due to the lower energies of its transition state (kinetic preference) and itself (thermodynamic preference). However, on Ag(110), the situation differs in two major aspects. On the one hand, the reactivity of the terminal alkynes is reported to be rather sensitive to the binding geometry.[32] Since the precursor and substrate employed in this study are different from those in the literature, a different mechanism may come into play due to the different surface binding geometry of the DEBPB precursor (kinetic effect). On the other hand, as described below, the Ag(110) surface lattice well matches the periodicity of the organometallic chain and hence lowers the total energy of the organometallic product on the surface (thermodynamic effect). As a result, the organometallic chains become the dominating products on Ag(110).

In fact, a perfect match between the periodicity of the 1D organometallic chain and the underlying Ag(110) lattice along the [001] direction was experimentally noticed. As shown in Figure 4d, the lattice stripes along the [1$\bar{1}$0] direction of the Ag(110) surface are clearly visible (highlighted by the dashed lines), and the organometallic chains orient along the [001] direction perpendicular to the [1$\bar{1}$0] stripes. A close look reveals that the Ag atoms in the organometallic chains exactly locate between two neighboring [1$\bar{1}$0] stripes, and two adjacent Ag atoms are separated by three stripes. This observation is consistent with the measured distance between two nearest Ag atoms in the organometallic chain, 1.24 ± 0.02 nm, which is coincidently three times that of the Ag(110) lattice

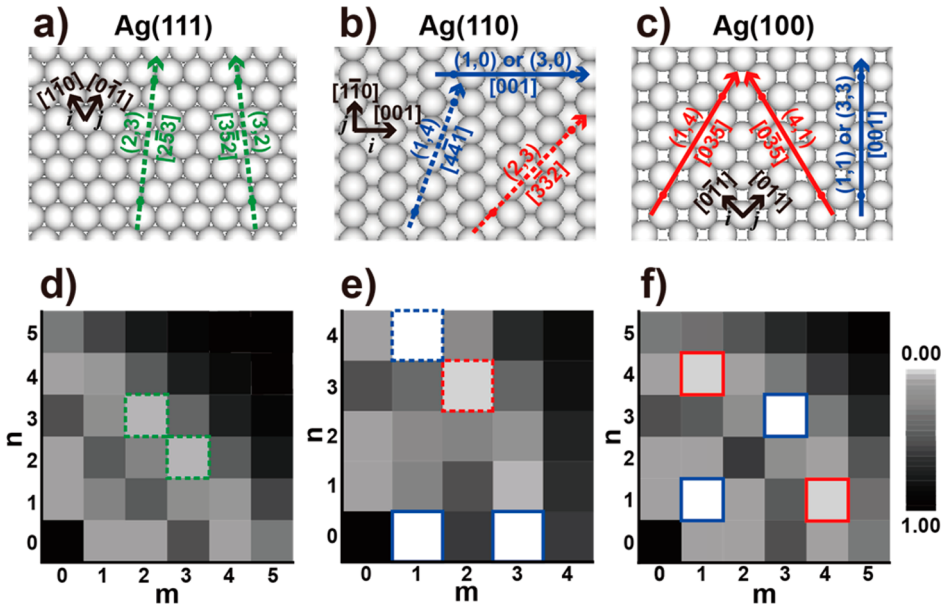

Figure 5. Surface lattice models of (a) Ag(111), (b) Ag(110), and (c) Ag(100). The base vectors i and j on each substrate are marked by black arrows. The directions whose lattice constants are a relatively good match with the periodicity of the organometallic chain are marked by colored arrows. Corresponding gray scale *K* maps are given for (d) Ag(111), (e) Ag(110), and (f) Ag(100). Encircled squares in different colors highlight the smallest or second smallest *K* values along the corresponding directions highlighted by the colored arrows in (a), (b), and (c).

periodicity (408.53 pm) along the [001] direction. The calculated model (Figure 4e) further confirms the perfect match between the periodicities of the organometallic chain and the Ag(110) lattice along the [001] direction, as shown by the dashed lines extended from Figure 4d. These findings point to hypothesis that the perfect match between the periodicities of the organometallic chain and the underlying Ag(110) lattice along the [001] direction may play a significant role in invoking a high selectivity of the organometallic reaction.

To elucidate the lattice match between the organometallic chain and substrate lattice on the selectivity of the organometallic reaction, the surface reaction of the DEBPB molecules on Ag(100) was also explored. To quantify the degree of lattice match between the periodicities along different directions on Ag(100) with that of the organometallic chain, a parameter, *K*, is defined below:[44]

$$K = \left| 1 - \frac{l|m\mathbf{i} + n\mathbf{j}|}{d} \right| \qquad (1)$$

where **i** and **j** are two basic vectors of the Ag(100) substrate, as marked by black arrows in Figure 5c, with *m* and *n* as their integer factors; *l* is an integer chosen to minimize *K*, and *d* is the periodicity of the organometallic chain (1.22 nm) obtained by theoretical optimization of its structure in vacuum. It should be pointed out that the *K* map is used to help understand the experimentally observed results. By no means can the *K* map be taken as a quantitative explanation based on DFT calculations.

By checking the *K* value at every point in the *m*−*n* coordinate, a map of matching degree between the periodicities of the organometallic chain and the Ag(100) substrate lattice along different orientations (termed as "*K* map") was obtained (Figure 5f). Obviously, the (*m*,*n*) points corresponding to the vectors whose lengths are much larger than the periodicity of the organometallic chain would lead to rather large *K* values. Therefore, only the (*m*,*n*) points corresponding to vectors whose lengths are smaller or around the periodicity of the organometallic chain are taken into account when the *K* map is drawn. According to eq 1, *K* is defined as the relative difference between the length of an arbitrary vector on the substrate and the periodicity of the organometallic chain. Therefore, the smaller the *K* value, the brighter the (*m*,*n*) square and the better the degree of lattice match. As a matter of fact, the *K* map and other similar methods[44−48] are frequently used to explain the formation of complicated structures along specific lattice directions on crystal substrates where DFT calculations of the total energy are not available.

In the *K* map of Ag(100) (Figure 5f), the two brightest squares are located at (1,1) and (3,3), as encircled by the blue squares in Figure 5f, corresponding to the [001] direction on Ag(100) (blue arrow in Figure 5c). The *K* value of these two points is 0.0070, which is rather close to zero, indicating a good match between the Ag(100) lattice along the [001] direction and the periodicity of the organometallic chain. This is not accidental because the [001] direction is simply that along which the organometallic chains on Ag(110)

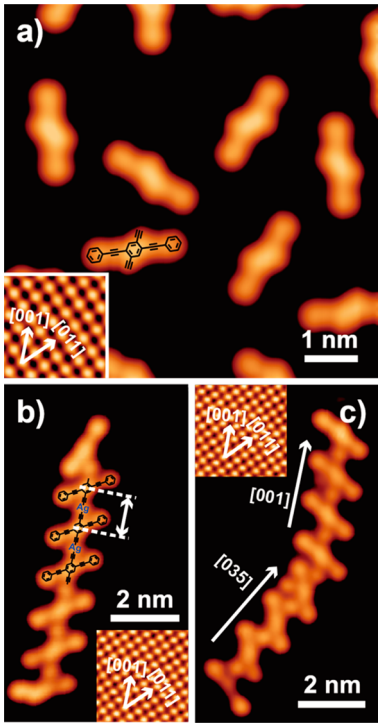

Figure 6. (a) STM image of the DEBPB molecules on Ag(100) with the chemical structure superimposed (0.01 V, 100 pA). Inset: High-resolution STM image of the Ag(100) surface lattice structure (0.01 V, 300 pA). (b) High-resolution STM image of an organometallic chain orienting along the [001] direction on Ag(100) with the chemical structure superimposed (0.01 V, 200 pA). The distance measured between the centers of two adjacent molecules is highlighted by the white arrow. Inset: High-resolution STM image of the Ag(100) surface lattice structure (0.01 V, 300 pA). (c) High-resolution STM image of an organometallic chain whose two bent segments orient along the [001] and [035] directions, respectively (0.01 V, 100 pA). Inset: High-resolution STM image of the Ag(100) surface lattice structure (0.01 V, 300 pA).

extend. Therefore, the same lattice match between the substrate lattice along [001] and periodicity of the organometallic chain on both Ag(100) and Ag(110) could be expected. Two other squares at (1,4) and (4,1) (encircled by the red squares in Figure 5f) correspond to [035] and [0$\bar{3}$5], respectively (red arrows in Figure 5c) and show the second smallest *K* value, 0.0214. As a result, the formation of the organometallic chains on Ag(100) and their orientations along [001] and even [035] (or [0$\bar{3}$5]) directions could be anticipated. This anticipation was confirmed by experimental observations. After deposition of the DEBPB monomers onto the Ag(100) substrate kept at about 100 K (Figure 6a) followed by subsequent annealing at about 320 K, 1D organometallic chains with the same chemical structure as that on Ag(110) were indeed captured (Supporting Information). High-resolution STM images of such anticipated organometallic chains are shown in Figure 6b,c. The organometallic species as suggested by the superimposed chemical structure in Figure 6b can be proven by the morphology and distance between the centers of two adjacent DEBPB molecules in the chain (1.20 ± 0.03 nm) which are similar to those of the organometallic ones on Ag(110). A careful comparison with the organometallic chain orientation on Ag(100) indicates that most chains extend along the [001] direction (Figure 6b), while a few others orient along the [035] (or [0$\bar{3}$5]) direction (Figure 6c). These experimental observations are in excellent agreement with those anticipated according to the *K* map. The productivities of the chains along different orientations, that is, the proportion of the molecules participating in the formation of the organometallic chains along different orientations, can be predicted to be dependent on match degree between the periodicity of the organometallic chain and the substrate lattice constant along a specific direction. With a better match along [001] (K = 0.0070), most organometallic products (about 84%) extend along the [001] direction. Meanwhile, with a poorer match along [035] (or [0$\bar{3}$5]) (K = 0.0214), only a very small fraction of the organometallic chains (about 16%) extends along the [035] (or [0$\bar{3}$5]) direction.

The *K* map can also be applied to explain the difference in surface reactions of the DEBPB molecules on Ag(111) and Ag(110). In the *K* map of Ag(111) (Figure 5d), two brightest squares, (2,3) and (3,2) (encircled by the dashed green squares in Figure 5d), corresponding to [2$\bar{5}$3] and [3$\bar{5}$2] directions, respectively, possess the smallest *K* value of about 0.0346 (marked by the dashed green arrows in Figure 5a). As a result, about 75% of organometallic segments formed on Ag(111) oriented along [2$\bar{5}$3], [3$\bar{5}$2], or other four equivalent directions. The remaining 25% oriented along other lattice directions because the orientation of an organometallic segment can be affected by the covalent connections. However, this relatively larger *K* value suggests a poor match between the organometallic chain periodicity and the underlying Ag(111) lattice constant, even though this is already the best match on Ag(111). Such a poor match implies that only a small productivity of the organometallic reaction (9%) exists on Ag(111), and short organometallic segments rather than extended long organometallic chains can be produced on Ag(111). In contrast, the [001] direction on Ag(110) (marked by the blue arrow in Figure 5b) along which the organometallic chains extend give rise to two brightest points, (1,0) and (3,0), with the smallest *K* value of 0.0070 in the *K* map of Ag(110) (highlighted by blue squares in Figure 5e). This finding confirms again that the perfect match between periodicity of the organometallic chains and the substrate lattice along the [001] direction leads to a high selectivity of the organometallic reaction on Ag(110). However, two other bright points in the *K* map of Ag(110), (1,4) (K = 0.0070, blue dashed square in Figure 5e) and (2,3) (K = 0.0214, red dashed square in Figure 5e), indicate that no organometallic chains are

produced to extend along these corresponding directions, [4$\bar{4}$1] and [3$\bar{3}$2] (dashed blue and red arrows in Figure 5b, respectively). The absence of the organometallic chains along these directions could be explained by the increase in the energy of the organometallic species along these directions caused by the change in location of the molecular backbone in the chains.

CONCLUSIONS

In summary, 1D covalent-bonded and organometallic molecular wires were prepared by the surface reactions of the DEBPB terminal alkyne precursor on both Ag(111) and Ag(110), respectively. Different lattice planes of the Ag substrate were employed to tune the reaction pathways and main products. Distinct reaction selectivities on Ag(111) and Ag(110) were revealed by STM observations, simulations, and theoretical MM and DFT calculations. On Ag(111), the Glaser coupling reaction dominated, leading to covalent-bonded chains with a productivity of 70%. On Ag(110), a high selectivity of the organometallic reaction was achieved, and the main product was highly oriented 1D silver−acetylide organometallic chains with a productivity of 88%. The effect of substrate lattices on the surface reactions of terminal alkynes, especially the high selectivity of the organometallic reaction on Ag(110), was explained by the specific stability of the organometallic products on Ag(110) caused by a perfect match between the periodicity of the organometallic chain and the substrate lattice constant. The impact of lattice match on the selectivity of the organometallic reaction was confirmed by the formation of the organometallic chains on Ag(100). All results could be well explained by the calculated and drawn *K* maps of Ag(111), Ag(110), and Ag(100). These findings provided the possibility of constructing surface structures by tuning reaction pathways of the precursors, such as terminal alkynes, with designed lattice structure of the employed substrate.

EXPERIMENT AND CALCULATION

All experiments were performed with a Unisoku UHV-STM with a base pressure better than 2×10^{-10} Torr in the system. The atomically flat crystalline Ag(111) and Ag(110) surfaces were prepared by repeated cycles of Ar^+ sputtering followed by annealing at about 780 K. DEBPB molecules (Supporting Information) were evaporated from a tantalum boat at about 420 K onto the clean substrates kept at about 100 K. The coverage of the molecules was controlled to be less than one monolayer. The samples were subsequently annealed at different temperatures. The substrate temperatures reported in this study were estimated based on the temperatures measured on the manipulator by referring to the temperature calibration curve of the substrate *versus* sample manipulator as supplied by the manufacturer. Therefore, the reported annealing temperatures could be lower than the actual ones. The STM tip was made out of an etched W wire (Ø 0.25 mm) and was prepared by E-beam heating in UHV. All STM images presented here were acquired at 4.2 K and in the constant current mode if not otherwise specifically stated. All STM images were processed by the WSxM software.[49]

Classical MM calculation based on MM2 force field[50] was used to optimize the position and orientation of the DEBPB monomer on Ag(111) and Ag(110) and the covalently coupled tetramer on Ag(111). The Ag(111) surface was constructed by a two atomic layer slab (960 atoms) of 56.4 Å × 57.6 Å in size, while the Ag(110) surface was built by a four atomic thick slab (1120 atoms) of 56.2 Å × 57.4 Å in size. All Ag atoms in these slabs were fixed during the calculations. The final position and structure of the monomers and tetramer were selected to minimize the total energy after scanning an area of 3 Å × 3 Å on Ag(111) (with a step of 0.03 Å) and of 10 Å × 10 Å on Ag(110) (with a step of 0.2 Å). At each position during the scan, the calculation was considered as converged when the total energy variation was smaller than 10^{-6} kcal/mol for two consecutive steps.

Since MM could not properly treat the organometallic compounds on metallic surfaces, we have performed DFT calculations by using the Vienna Ab Initio Simulation Package (VASP),[51,52] with pseudopotentials described by the projector-augmented wave method.[53] The exchange-correlation energy was calculated within the generalized gradient approximation and functional proposed by Perdew−Burke−Ernzerhof.[54,55] The kinetic energy cutoff was set to 460 eV. The optimized lattice parameter of the face-centered cubic silver was 4.162 Å by using a 13 × 13 × 13 Monkhorst−Pack mesh[56] for the Brillouin zone. The van der Waals dispersive correction was considered for intramolecular, intermolecular, and molecule−substrate interactions with the DFT-D2 method[57] as implemented in VASP. For the adsorption of an organometallic dimer, the Ag(111) surface was described by a four atomic layers slab of 168 atoms. The dimension of the supercell was 25.6 Å × 15.3 Å × 27.4 Å. The Ag(110) surface was modeled by a four atomic layers slab of 240 atoms within a 25.0 Å × 29.4 Å × 20.1 Å supercell. Due to the large dimension of these supercells, only the Γ point was used for the Brillouin zone sampling. During the optimization, except for the Ag atoms in the two bottom layers of the slabs that were fixed, all other atoms were relaxed until the force on each of them was smaller than 50 meV/Å. The electronic self-consistent field (SCF) step was converged within 1 meV.

STM images were simulated using GREEN,[58] a program based on extended Hückel theory.[59] The substrate−molecule−STM tip junction was explicitly described. The geometry and position of the DEBPB monomer and its organometallic/covalent oligomers were obtained by MM or DFT calculations (except for the geometry of the organometallic tetramer, which was extrapolated from the optimized organometallic dimer's geometry). Depending on the size of the molecule, we adopted different surface unit cells from 7 × 9 up to 15 × 19. The W(111) STM tip was terminated by an apex of 10 atoms. At each (*x*,*y*,*z*) position of the tip, the transmission coefficient was evaluated through a Greens function approach, and the tunneling current was calculated by applying the Landauer−Büttiker formula.[60] All STM simulations were processed by the WSxM software.

Conflict of Interest: The authors declare no competing financial interest.

Acknowledgment. This work was jointly supported by NSFC (21133001, 21333001, 21261130090, 21433011, 61321001, 913000002) and MOST (2013CB933404, 2011CB808702), China. Partial support from the Singapore NRF CREATE-SPURc project is also acknowledged.

Supporting Information Available: Preparation methods of DEBPB. Explanation and proof of the creation of a CO-modified tip. STM images of products on Ag(110) at higher annealing temperatures. Statistics on the productivity of reaction products on Ag(111), Ag(110), and Ag(100). The Supporting Information is available free of charge on the ACS Publications website at DOI: 10.1021/acsnano.5b01803.

REFERENCES AND NOTES

1. Champness, N. R. Building with Molecules. *Nat. Nanotechnol.* **2007**, *2*, 671–672.
2. Grill, L.; Dyer, M.; Lafferentz, L.; Persson, M.; Peters, M. V.; Hecht, S. Nano-Architectures by Covalent Assembly of Molecular Building Blocks. *Nat. Nanotechnol.* **2007**, *2*, 687–691.
3. Gourdon, A. On-Surface Covalent Coupling in Ultrahigh Vacuum. *Angew. Chem., Int. Ed.* **2008**, *47*, 6950–6953.
4. Champness, N. R. Surface Chemistry: Making the Right Connections. *Nat. Chem.* **2012**, *4*, 149–150.
5. Lafferentz, L.; Eberhardt, V.; Dri, C.; Africh, C.; Comelli, G.; Esch, F.; Hecht, S.; Grill, L. Controlling On-Surface Polymerization by Hierarchical and Substrate-Directed Growth. *Nat. Chem.* **2012**, *4*, 215–220.
6. Colson, J. W.; Dichtel, W. R. Rationally Synthesized Two-Dimensional Polymers. *Nat. Chem.* **2013**, *5*, 453–465.
7. Elemans, J. A. A. W.; Lei, S.; De Feyter, S. Molecular and Supramolecular Networks on Surfaces: From Two-Dimensional Crystal Engineering to Reactivity. *Angew. Chem., Int. Ed.* **2009**, *48*, 7298–7332.
8. Perepichka, D. F.; Rosei, F. Extending Polymer Conjugation into the Second Dimension. *Science* **2009**, *323*, 216–217.
9. Sakamoto, J.; van Heijst, J.; Lukin, O.; Schluter, A. D. Two-Dimensional Polymers: Just a Dream of Synthetic Chemists? *Angew. Chem., Int. Ed.* **2009**, *48*, 1030–1069.
10. Palma, C.-A.; Samorì, P. Blueprinting Macromolecular Electronics. *Nat. Chem.* **2011**, *3*, 431–436.
11. Hla, S.-W.; Bartels, L.; Meyer, G.; Rieder, K.-H. Inducing All Steps of a Chemical Reaction with the Scanning Tunneling Microscope Tip: Towards Single Molecule Engineering. *Phys. Rev. Lett.* **2000**, *85*, 2777–2780.
12. Bieri, M.; Treier, M.; Cai, J.; Ait-Mansour, K.; Ruffieux, P.; Groning, O.; Groning, P.; Kastler, M.; Rieger, R.; Feng, X.; et al. Porous Graphenes: Two-Dimensional Polymer Synthesis with Atomic Precision. *Chem. Commun.* **2009**, 6919–6921.
13. Lafferentz, L.; Ample, F.; Yu, H.; Hecht, S.; Joachim, C.; Grill, L. Conductance of a Single Conjugated Polymer as a Continuous Function of Its Length. *Science* **2009**, *323*, 1193–1197.
14. Bieri, M.; Nguyen, M.-T.; Gröning, O.; Cai, J.; Treier, M.; Aït-Mansour, K.; Ruffieux, P.; Pignedoli, C. A.; Passerone, D.; Kastler, M.; et al. Two-Dimensional Polymer Formation on Surfaces Insight into the Roles of Precursor Mobility and Reactivity. *J. Am. Chem. Soc.* **2010**, *132*, 16669–16676.
15. Cai, J.; Ruffieux, P.; Jaafar, R.; Bieri, M.; Braun, T.; Blankenburg, S.; Muoth, M.; Seitsonen, A. P.; Saleh, M.; Feng, X.; et al. Atomically Precise Bottom-Up Fabrication of Graphene Nanoribbons. *Nature* **2010**, *466*, 470–473.
16. Zwaneveld, N. A. A.; Pawlak, R.; Abel, M.; Catalin, D.; Gigmes, D.; Bertin, D.; Porte, L. Organized Formation of 2D Extended Covalent Organic Frameworks at Surfaces. *J. Am. Chem. Soc.* **2008**, *130*, 6678–6679.
17. Zhong, D.; Franke, J. H.; Podiyanachari, S. K.; Blomker, T.; Zhang, H.; Kehr, G.; Erker, G.; Fuchs, H.; Chi, L. Linear Alkane Polymerization on a Gold Surface. *Science* **2011**, *334*, 213–216.
18. Matena, M.; Riehm, T.; Stöhr, M.; Jung, T. A.; Gade, L. H. Transforming Surface Coordination Polymers into Covalent Surface Polymers: Linked Polycondensed Aromatics through Oligomerization of N-Heterocyclic Carbene Intermediates. *Angew. Chem., Int. Ed.* **2008**, *47*, 2414–2417.
19. Okawa, Y.; Aono, M. Nanoscale Control of Chain Polymerization. *Nature* **2001**, *409*, 683–684.
20. Sullivan, S. P.; Schnieders, A.; Mbugua, S. K.; Beebe, T. P., Jr. Controlled Polymerization of Substituted Diacetylene Self-Organized Monolayers Confined in Molecule Corrals. *Langmuir* **2005**, *21*, 1322–1327.
21. Okawa, Y.; Aono, M. Linear Chain Polymerization Initiated by a Scanning Tunneling Microscope Tip at Designated Positions. *J. Chem. Phys.* **2001**, *115*, 2317–2322.
22. Sun, Q.; Zhang, C.; Li, Z.; Kong, H.; Tan, Q.; Hu, A.; Xu, W. On-Surface Formation of One-Dimensional Polyphenylene through Bergman Cyclization. *J. Am. Chem. Soc.* **2013**, *135*, 8448–8451.
23. Wang, W.; Shi, X.; Wang, S.; Van Hove, M. A.; Lin, N. Single-Molecule Resolution of an Organometallic Intermediate in a Surface-Supported Ullmann Coupling Reaction. *J. Am. Chem. Soc.* **2011**, *133*, 13264–13267.
24. Chung, K. H.; Koo, B. G.; Kim, H.; Yoon, J. K.; Kim, J. H.; Kwon, Y. K.; Kahng, S. J. Electronic Atructures of One-Dimensional Metal-Molecule Hybrid Chains Studied Using Scanning Tunneling Microscopy and Density Functional Theory. *Phys. Chem. Chem. Phys.* **2012**, *14*, 7304–7308.
25. Giovannantonio, M. D.; Garah, M. E.; Lipton-Duffin, J.; Meunier, V.; Cardenas, L.; Revurat, Y. F.; Cossaro, A.; Contini, G. Insight into Organometallic Intermediate and Its Evolution to Covalent Bonding in Surface-Confined Ullmann Polymerization. *ACS Nano* **2013**, *7*, 8190–8198.
26. Hanke, F.; Haq, S.; Raval, R.; Persson, M. Heat-to-Connect Surface Commensurability Directs Organometallic One-Dimensional Self-Assembly. *ACS Nano* **2011**, *5*, 9093–9103.
27. Haq, S.; Hanke, F.; Dyer, M. S.; Persson, M.; Iavicoli, P.; Amabilino, D. B.; Raval, R. Clean Coupling of Unfunctionalized Porphyrins at Surfaces To Give Highly Oriented Organometallic Oligomers. *J. Am. Chem. Soc.* **2011**, *133*, 12031–21039.
28. Haq, S.; Hank, F.; Sharp, J.; Persson, M.; Amabilino, D. B.; Raval, R. Versatile Bottom-Up Construction of Diverse Macromolecules on a Surface Observed by Scanning Tunneling Microscopy. *ACS Nano* **2014**, *8*, 8856–8870.
29. Glaser, C. A. Beiträge zur Kenntniss des Acetenylbenzols. *Ber. Dtsch. Chem. Ges.* **1869**, *2*, 422–424.
30. Glaser, C. Untersuchungen über einige Derivate der Zimmtsäure. *Ann. Chem. Pharm.* **1870**, *154*, 137–171.
31. Li, G.; Li, Y.; Liu, H.; Guo, Y.; Lia, Y.; Zhu, D. Architecture of Graphdiyne Nanoscale Films. *Chem. Commun.* **2010**, *46*, 3256–3258.
32. Zhang, Y. Q.; Kepcija, N.; Kleinschrodt, M.; Diller, K.; Fischer, S.; Papageorgiou, A. C.; Allegretti, F.; Bjork, J.; Klyatskaya, S.; Klappenberger, F.; et al. Homo-coupling of Terminal Alkynes on a Noble Metal Surface. *Nat. Commun.* **2012**, *3*, 1286.
33. Gao, H. Y.; Wagner, H.; Zhong, D.; Franke, J. H.; Studer, A.; Fuchs, H. Glaser Coupling at Metal Surfaces. *Angew. Chem., Int. Ed.* **2013**, *52*, 4024–4028.
34. Gao, H.-Y.; Franke, J.-H.; Wagner, H.; Zhong, D.; Held, P.-A.; Studer, A.; Fuchs, H. Effect of Metal Surfaces in On-Surface Glaser Coupling. *J. Phys. Chem. C* **2013**, *117*, 18595–18602.
35. Björk, J.; Zhang, Y.-Q.; Klappenberger, F.; Barth, J. V.; Stafström, S. Unraveling the Mechanism of the Covalent Coupling between Terminal Alkynes on a Noble Metal. *J. Phys. Chem. C* **2014**, *118*, 3181–3187.
36. Cirera, B.; Zhang, Y. Q.; Björk, J.; Klyatskaya, S.; Chen, Z.; Ruben, M.; Barth, J. V.; Klappenberger, F. Synthesis of Extended Graphdiyne Wires by Vicinal Surface Templating. *Nano Lett.* **2014**, *14*, 1891–1897.
37. Gao, H.-Y.; Zhong, D.; Mönig, H.; Wagner, H.; Held, P.-A.; Timmer, A.; Studer, A.; Fuchs, H. Photochemical Glaser Coupling at Metal Surfaces. *J. Phys. Chem. C* **2014**, *118*, 6272–6277.
38. Liu, J.; Ruffieux, P.; Feng, X.; Müllen, K.; Fasel, R. Cyclotrimerization of Arylalkynes on Au(111). *Chem. Commun.* **2014**, *50*, 11200–11203.
39. Zhou, H.; Liu, J.; Du, S.; Zhang, L.; Li, G.; Zhang, Y.; Tang, B. Z.; Gao, H. J. Direct Visualization of Surface-Assisted Two-Dimensional Diyne Polycyclotrimerization. *J. Am. Chem. Soc.* **2014**, *136*, 5567–5570.
40. Eichhorn, J.; Heckl, W. M.; Lackinger, M. On-Surface Polymerization of 1,4-Diethynylbenzene on Cu(111). *Chem. Commun.* **2013**, *49*, 2900–2902.
41. Ecija, D.; Vijayaraghavan, S.; Auwärter, W.; Joshi, S.; Seufert, K.; Aurisicchio, C.; Bonifazi, D.; Barth, J. V. Two-Dimensional Short-Range Disordered Crystalline Networks from Flexible Molecular Modules. *ACS Nano* **2012**, *6*, 4258–4265.
42. Fan, Q.; Wang, C.; Han, Y.; Zhu, J.; Kuttner, J.; Hilt, G.; Gottfried, J. M. Surface-Assisted Formation, Assembly, and Dynamics of Planar Organometallic Macrocycles and

Zigzag Shaped Polymer Chains with C−Cu−C Bonds. *ACS Nano* **2014**, *8*, 709–718.
43. Eichhorn, J.; Strunskus, T.; Rastgoo-Lahrood, A.; Samanta, D.; Schmittel, M.; Lackinger, M. On-Surface Ullmann Polymerization *via* Intermediate Organometallic Networks on Ag(111). *Chem. Commun.* **2014**, *50*, 7680–7682.
44. Schull, G.; Berndt, R. Orientationally Ordered (7 × 7) Superstructure of C_{60} on Au(111). *Phys. Rev. Lett.* **2007**, *99*, 226105.
45. Enachescu, M.; Schleef, D.; Ogletree, D. F.; Salmeron, M. Integration of Point-Contact Microscopy and Atomic-Force Microscopy: Application to Characterization of Graphite/Pt(111). *Phys. Rev. B* **1999**, *60*, 16913–16919.
46. Qin, Z.; Liu, C.; Chen, J.; Guo, Q.; Yu, Y.; Cao, G. Molecular Orientation and Lattice Ordering of C_{60} Molecules on the Polar FeO/Pt(111) Surface. *J. Chem. Phys.* **2012**, *136*, 024701.
47. Hillier, A. C.; Ward, M. D. Epitaxial Interactions between Molecular Overlayers and Ordered Substrates. *Phys. Rev. B* **1996**, *54*, 14037–14051.
48. Hooks, D. E.; Fritz, T.; Ward, M. D. Epitaxy and Molecular Organization on Solid Substrates. *Adv. Mater.* **2001**, *13*, 227–241.
49. Horcas, I.; Fernandez, R.; Gomez-Rodriguez, J. M.; Colchero, J.; Gomez-Herrero, J.; Baro, A. M. WSXM: A Software for Scanning Probe Microscopy and a Tool for Nanotechnology. *Rev. Sci. Instrum.* **2007**, *78*, 013705.
50. Allinger, N. L. Conformational Analysis. 130. MM2. A Hydrocarbon Force Field Utilizing V_1 and V_2 Torsional Terms. *J. Am. Chem. Soc.* **1977**, *99*, 8127–8134.
51. Kresse, G.; Furthmüller, J. Efficient Iterative Schemes for *Ab Initio* Total-Energy Calculations Using a Plane-Wave Basis Set. *Phys. Rev. B* **1996**, *54*, 11169–11186.
52. Kresse, G.; Hafner, J. *Ab Initio* Molecular Dynamics for Liquid Metals. *Phys. Rev. B* **1993**, *47*, 558–561.
53. Blöchl, P. E. Projector Augmented-Wave Method. *Phys. Rev. B* **1994**, *50*, 17953–17979.
54. Perdew, J.; Burke, K.; Ernzerhof, M. Generalized Gradient Approximation Made Simple. *Phys. Rev. Lett.* **1996**, *77*, 3865–3868.
55. Perdew, J.; Burke, K.; Ernzerhof, M. Generalized Gradient Approximation Made Simple. *Phys. Rev. Lett.* **1997**, *78*, 1396–1396.
56. Monkhorst, H. J.; Pack, J. D. Special Points for Brillouin-Zone Integrations. *Phys. Rev. B* **1976**, *13*, 5188–5192.
57. Grimme, S. Semiempirical GGA-Type Density Functional Constructed with a Long-Range Dispersion Correction. *J. Comput. Chem.* **2006**, *27*, 1787–1799.
58. Cerdá, J.; Van Hove, M.; Sautet, P.; Salmeron, M. Efficient Method for the Simulation of STM Images. I. Generalized Green-Function Formalism. *Phys. Rev. B* **1997**, *56*, 15885–15899.
59. Cerdá, J.; Soria, F. Accurate and Transferable Extended Hückel-Type Tight-Binding Parameters. *Phys. Rev. B* **2000**, *61*, 7965–7971.
60. Büttiker, M.; Imry, Y.; Landauer, R.; Pinhas, S. Generalized Many-Channel Conductance Formula with Application to Small Rings. *Phys. Rev. B* **1985**, *31*, 6207–6215.